



HAL
open science

A benchmarking study of Geant4 for Auger electrons emitted by medical radioisotopes

Samer Bakr, Tibor Kibédi, Bryan Tee, David Bolst, Maarten Vos, Mohammed Alotiby, Laurent Desorgher, Dennis Herbert Wright, Alfonso Mantero, Anatoly Rosenfeld, et al.

► To cite this version:

Samer Bakr, Tibor Kibédi, Bryan Tee, David Bolst, Maarten Vos, et al.. A benchmarking study of Geant4 for Auger electrons emitted by medical radioisotopes. *Applied Radiation and Isotopes*, 2021, 174, pp.109777. 10.1016/j.apradiso.2021.109777 . hal-03237846

HAL Id: hal-03237846

<https://hal.science/hal-03237846>

Submitted on 7 Jun 2021

HAL is a multi-disciplinary open access archive for the deposit and dissemination of scientific research documents, whether they are published or not. The documents may come from teaching and research institutions in France or abroad, or from public or private research centers.

L'archive ouverte pluridisciplinaire **HAL**, est destinée au dépôt et à la diffusion de documents scientifiques de niveau recherche, publiés ou non, émanant des établissements d'enseignement et de recherche français ou étrangers, des laboratoires publics ou privés.

A benchmarking study of Geant4 for Auger electrons emitted by medical radioisotopes

Samer Bakr^a, Tibor Kibédi^b, Bryan Tee^b, David Bolst^a, Maarten Vos^c, Mohammed Alotiby^d, Laurent Desorgher^e, Dennis Herbert Wright^{f,g}, Alfonso Mantero^h, Anatoly Rosenfeld^{a,i}, Vladimir Ivanchenko^{j,k}, Sebastien Incerti^{l,m}, Susanna Guatelli^{a,i}

^a Centre for Medical Radiation Physics, University of Wollongong, Wollongong, Australia

^b Department of Nuclear Physics, Research School of Physics, The Australian National University, Canberra, Australia

^c Electronic Materials Engineering, Research School of Physics, The Australian National University, Canberra, Australia

^d King Abdulaziz City for Science and Technology, Riyadh, Saudi Arabia

^e Lausanne University Hospital, Lausanne, Switzerland

^f International Space Elevator Consortium, California, USA

^g SLAC National Accelerator Laboratory, California, USA

^h SWHARD s.r.l.

ⁱ Illawarra Health and Medical Research Institute, University of Wollongong, Wollongong, Australia

^j Geant4 Associates International Ltd.

^k Tomsk State University, Tomsk, Russia

^l CNRS/IN2P3, Centre d'Etudes Nucléaires de Bordeaux-Gradignan, Bordeaux, France

^m Université de Bordeaux, Bordeaux, France

Abstract

Auger emitting radioisotopes are of great interest in targeted radiotherapy because, once internalised in the tumour cells, they can deliver dose locally to the radiation sensitive targets, while not affecting surrounding cells. Geant4 is a Monte Carlo code widely used to characterise the physics mechanism at the basis of targeted radiotherapy. In this work, we benchmarked the modelling of the emission of Auger electrons in Geant4 deriving from the decay of ¹²³I, ¹²⁴I, ¹²⁵I radionuclides against existing theoretical approaches. We also compared Geant4 against reference data in the case of ¹³¹Cs, which is of interest for brachytherapy. In the case of ¹²⁵I and ¹³¹Cs, the simulation results are compared to experimental measurements as well. Good agreement was found between Geant4 and the reference data. As far as we know, this is the first study aimed to benchmark against experimental measurements the emission of Auger electrons in Geant4 for radiotherapy applications.

Keywords

Auger electron, radioactive decay, Monte Carlo, Geant4.

1. Introduction

The Auger effect involves the emission of atomic electrons as alternative channel to X-ray fluorescence in the atomic de-excitation, which follows the creation of a vacancy in an atomic

39 shell [1], [2]. Auger electron emitting radionuclides are of great interest in targeted
40 radiotherapy because Auger electrons have high Linear Energy Transfer (4–26 keV/μm) and
41 short range [3]–[6].

42 The present paper reports on the Auger electron emission following the radioactive decay of
43 ^{123}I , ^{124}I , ^{125}I and ^{131}Cs . The iodine radioisotopes are widely used in nuclear medicine for the
44 labelling of monoclonal antibodies, receptors and other radio-pharmaceuticals, especially in
45 diagnostic and therapeutic applications, where quantitative imaging over a period of several
46 days is necessary [7]–[9]. The optimal combination of half-life and energy of the emitted
47 radiation makes ^{131}Cs an attractive radioisotope for brachytherapy of malignant tumours.

48 Geant4 [10] is a Monte Carlo code which is extensively used in medical physics applications,
49 including micro- and nano- dosimetry [11], [12], brachytherapy and targeted radiotherapy
50 [13], [14]. Therefore, it is important to benchmark the emission of Auger electrons in Geant4
51 against reference data.

52 The goal of this work is to benchmark, for the first time, Geant4 in terms of emission of Auger
53 electrons. A Geant4 simulation was developed to calculate the emission yields and energy
54 spectra of Auger electrons emitted from ^{123}I , ^{124}I , ^{125}I and ^{131}Cs radionuclides. The results were
55 compared to other Monte Carlo based calculations available in the literature and
56 experimental measurements performed at the Australian National University (ANU) and the
57 Joint Institute for Nuclear Research (JINR) in the case of ^{125}I and ^{131}Cs , respectively.

58 **2. Materials and methods**

59 **2.1. Radioactive decays under investigation**

60 ^{123}I (half-life $T_{1/2} = 13.224$ hr) decays by electron capture (EC) (100% probability) to an excited
61 state of ^{123}Te . The strongest transition at 159 keV carries 99% of the total intensity and 19%
62 of the time will decay via internal conversion (IC) to ^{123}Te , which has a very long half-life ($T_{1/2}$
63 $= 9.2 \times 10^{16}$ year) [15].

64 ^{124}I ($T_{1/2} = 4.176$ d) decays via either β^+ (22.7% probability) or EC (77.3% probability) to either
65 excited states (65% probability) or to the ground state (35% probability) of ^{124}Te [16].

66 ^{125}I ($T_{1/2} = 59.49$ d) decays by EC (100% probability) followed by either gamma ray emission
67 (6.68% probability) or IC (93.32% probability), to the ground state of the stable ^{125}Te [17].

68 ^{131}Cs decays directly via EC decay to the ground state of ^{131}Xe , hence, Auger electrons are only
69 emitted from the atomic relaxation in ^{131}Xe from the vacancy created by EC. ^{131}Cs is one of
70 the pure Auger emitters for nuclear medicine [18].

71 **2.2. Atomic Relaxation in Geant4**

72 Geant4 has the functionality of simulating both the radiative (X-ray) and non-radiative (Auger)
73 atomic relaxation process of singly ionised atoms [19], [20]. Geant4 treats ionised atoms as
74 isolated entities [21]. This means that an atom exists separately without bonding with any
75 other atom. The creation of a vacancy is handled by the Geant4 electromagnetic physics
76 package. The generation of the relaxation cascade is handled by the atomic relaxation
77 component, which is used by all the primary processes generating a vacancy [19], [20], [22].
78 The simulation of atomic relaxation takes place in two stages:

79 1) determination of the shell (or sub-shell) where the vacancy is created by the primary
80 process, radioactive decay in this case;

81 2) the relaxation cascade is then triggered, starting from the vacancy created by the
82 primary process; secondary photons or electrons are generated through radiative and
83 non-radiative transitions, based on the respective transition probabilities [19]–[22].

84 In stage 1, the *G4RadioactiveDecay* module is used to simulate the decay, either at rest or in-
85 flight, of radioactive nuclei by electron capture (EC) and by α , β^- and β^+ emission or isomeric
86 (IT) decay. If the daughter of a nuclear decay is an excited isomer, its prompt nuclear de-
87 excitation is treated using the *G4PhotoEvaporation* class [10].

88 The subshell ratios for electron capture is calculated according to Bambynek [23]. In this
89 model only electrons from the $s_{1/2}$ and $p_{1/2}$ subshells (K, L1-L2, M1-M2, N1-N2) are captured.
90 Whereas, for internal conversion the probabilities are specified in Geant4
91 *PhotoEvaporation5.5* data library (version used in this work). These probabilities are
92 computed with BRICC code [24], except if they are provided in the ENSDF files.

93 Geant4 uses the Livermore Evaluation Atomic Data Library EADL [21] in stage 2 to calculate
94 the complete radiative and non-radiative emission of X-rays and Auger electrons as the atom
95 relaxes [10]. The energy of the relaxation product is calculated as the difference of the sub-
96 shell binding energies involved with the atomic de-excitation process [21]. It is assumed that
97 the binding energy of all subshells are the same for neutral ground state atoms as for ionised
98 atoms [10], [21]. The Geant4 Atomic Relaxation model does not distinguish between Auger
99 and Coster-Kronig transitions [20], thus, the term Auger is used for both transitions.

100 2.3. Geant4 simulation setup

101 The Geant4 extended example *rdecay01* was used in this study and Geant4 10.05.p01 version
102 has been adopted. A cube of 20 mm size of vacuum is modelled, with a point source of ^{123}I ,
103 ^{124}I , ^{125}I and ^{131}Cs in the centre of the box. The radioactive decay and the full atomic relaxation
104 are modelled. The output of the simulation is the emission yield per radioactive decay and
105 the energy spectra of the emitted Auger electrons. The number of histories in the Geant4
106 simulation is 10^7 to obtain a statistical uncertainty below 1%. Nevertheless, it should be noted
107 that the uncertainty of EADL Auger electrons yields for an inner shell vacancy is less than 15%
108 [21]. Only inner shell vacancies are considered in this work when comparing the simulation
109 results to experimental data. The calculated Auger electron spectra were binned using 50 eV
110 bin width. In the analysis of the results, the Auger electrons have been grouped according to
111 the IUPAC notation, based on the atomic shells involved in the transition [25]. Following this
112 notation, Auger MXY, M-shell Auger transition where neither of the two new vacancies is in
113 the N-shell. Auger LMX, L-shell Auger transition where one of the vacancies is in the M-shell.
114 Auger LMM, L-shell Auger transition where both new vacancies are in the M-shell. Auger KLL,
115 K-shell Auger transition where both new vacancies are in the L-shell. Auger KLX, K-shell Auger
116 transition where one of the two new vacancies is in the L-shell. And Auger KXY, K-shell Auger
117 transition where neither of the two new vacancies is in the L-shell.

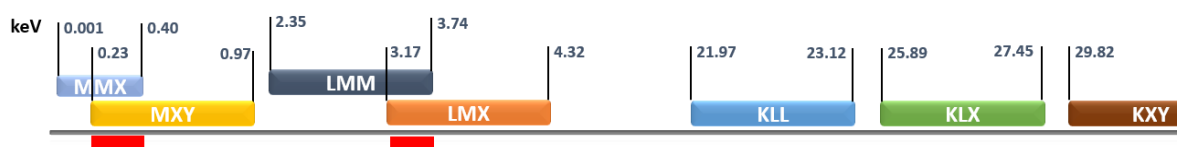


Fig. 1 Energy ranges for Auger electron groups in tellurium according to EADL [21].
Overlapping energy ranges are indicated with red squares below the axis.

118 Each individual Auger electron energy line calculated by means of the Geant4 simulation
 119 needs to be associated to the specific transition producing it, as this information is not
 120 provided automatically in a Geant4 user application. This method has been adopted as
 121 currently it is not possible to directly retrieve the transition type in a Geant4 user application.
 122 In the analysis of the simulation results, Auger KLL, KLX, and KXY lines were grouped according
 123 to their energy ranges in EADL [21], as shown in Fig. 1 (e.g., the line 3.6185 keV matches with
 124 L2M1O3 transition energy (EADL [21]), so it belongs to group LMX). To note, the Geant4
 125 simulation results showed a slight energy broadening of the Auger lines due to momentum
 126 transfer to the daughter of the radioactive decay. When we find two transitions for the same
 127 energy in overlapping energy ranges as represented in Fig. 1, the difficulty to retrieve the
 128 transition shows up. This problem is due to the fact that the bin width in the simulation is 1
 129 eV, which is greater than the difference between a few transition energies (e.g., the line
 130 L3M5M5 3.17422 keV and L3M1N1 3.17429 keV (EADL [21])). In these situations, we decided
 131 to choose the most probable transition for the specific line.

132 The mean energy, \bar{E} of each Auger transition groups (MXY, LMM, LMX, KLL, KLX and KXY) was
 133 evaluated as:

$$134 \quad \bar{E} = \frac{\sum_i (E_i \cdot Y_i)}{Y_{Total}}, \quad (\text{equation 1})$$

135

136 where E_i is the energy and Y_i is the yield of an Auger line in the group. Y_{Total} is the total yield
 137 of the Auger group.

138 **2.4. Theoretical approaches used to benchmark Geant4 atomic relaxation**

139 The theoretical approaches used to benchmark Geant4 are based on the Monte Carlo based
 140 calculations by Pomplun [26], Stepanek [27] and the BrIccEmis by Lee et al., developed at the
 141 Australian National University (ANU) [3], [4], [28], [29]. Table 1 summarises the models and
 142 data libraries used in the calculations. In the BrIccEmis calculations the so-called “isolated
 143 atom” approximation was used, namely once a vacancy reached the valence shell, it remained
 144 unfilled.

145 *Table 1. Atomic and nuclear data used in the calculations by Stepanek [27], Pomplun [26]*
 146 *and in BrIccEmis [4], as well as in Geant4.*

	Stepanek [27]	Pomplun [26]	BrIccEmis [4]	Geant4
Nuclear decay data	ENSDF [30]	ICRP38 [31]	ENSDF [30]	ENSDF [30]
Electron capture probabilities	Gove <i>et al.</i> [32] Martin <i>et al.</i> [33]	Gove <i>et al.</i> [32]	Schönfeld [34]	Bambynek <i>et al.</i> [23]
Atomic shells	K-N	K-N	K-O	K-O

Atomic transition rates	Perkins <i>et al.</i> (EADL) [21]	Storm <i>et al.</i> [35] Chen <i>et al.</i> [36] McGuire <i>et al.</i> [37]	Perkins <i>et al.</i> (EADL) [21]	Perkins <i>et al.</i> (EADL) [21]
Atomic transition energies	Dirac-Hartree-Slater [38]	Dirac-Fock Deslaux [39]	Dirac-Fock Band <i>et al.</i> [40]	Perkins <i>et al.</i> (EADL) [21]

147

148 The yields of Auger electron emission have been calculated as described in Section 2.3 and
 149 also computed analytically (called here *Geant4Lib analytical code*) by using directly the
 150 radioactive decay, nuclear de-excitation, and atomic relaxation data contained in the Geant4
 151 data libraries. This approach allows to verify that the input data libraries are used correctly by
 152 the Geant4 kernel when performing simulations of radioactive decay.

153 In the Geant4lib analytical code, the yield of a given Auger electron line is obtained by the
 154 sum of the probabilities of the different disintegration branches leading to the emission of
 155 this specific line. Each disintegration branch consists in the succession of a radioactive
 156 disintegration of the parent nucleus to an excited state of the daughter, a cascade of nuclear
 157 deexcitation with at least one electron conversion emission, and an atomic relaxation cascade
 158 leading to the emission of the considered Auger line. The probability of a branch is obtained
 159 by the product of the probability of all steps involved in the branch. This code does not take
 160 into account the nuclear recoil broadening, which is instead considered in the full Geant4
 161 simulation used in this work.

162 **2.5. Reference experimental measurements**

163 Two sets of experimental measurements of Auger electron spectra were used in this work.
 164 The first set derives from experimental measurement with an ^{125}I source performed at the
 165 ANU obtained with an electron momentum spectrometer (EMS) which can measure electrons
 166 from 2 keV to 40 keV (the energy resolution of the spectrometer is ≈ 6 eV) [8]. The iodine
 167 source was prepared at ANSTO (Australia’s Nuclear Science and Technology Organisation)
 168 with a NaI solution deposited on top of a $200 \mu\text{g}/\text{cm}^2$ gold substrate, following the procedure
 169 described by Pronschinske *et al* [41]. The resulting source was a monolayer of ^{125}I on top of
 170 the gold substrate [42].

171 The second set of experimental measurements is documented in [43]. A BaCO_3 target was
 172 irradiated in the nuclear reactor IBR-2 of the JINR lab, Dubna, at the neutron flux of
 173 $\sim 2.5 \times 10^{12} \frac{n}{\text{cm}^2.s}$ for 10 days. The electron spectrum was measured using a combined
 174 electrostatic spectrometer [44], consisting of a retarding sphere followed by a double-pass
 175 cylindrical mirror energy analyser [43].

176 Table 2 summarises the radioisotopes under study and the reference theoretical and
 177 experimental data used to benchmark Geant4.

178 *Table 2. List of reference published data used in this study. We compare only K-lines in the*
 179 *case of validation against experimental data.*

	Calculations	Experimental
^{123}I	BrlccEmis [4] Pomplun [45]	-
^{124}I	BrlccEmis [4]	-
^{125}I	BrlccEmis [4] Stepanek [27] Pomplun (KLL spectrum) [26]	ANU (KLL spectrum) [8]
^{131}Cs	-	JINR (KLL spectrum) [43]

180

181 **3. Results**

182 The first section shows the comparison of Geant4 results against the theoretical predictions
 183 by BrlccEmis [4], [29], Pomplun [26], [45] and Stepanek [27] for ^{123}I , ^{124}I and ^{125}I in terms of
 184 emission yields of Auger electrons. The second section is dedicated to the comparison against
 185 experimental measurements for ^{125}I and ^{131}Cs radioisotopes.

186 **3.1. Comparison to other theoretical approaches**

187 Fig. 2, 3 and 4 present the generated energy spectra and yield of Auger electrons for ^{123}I , ^{124}I
 188 and ^{125}I decays, respectively, using the Geant4 simulation described in Section 2.3 and
 189 BrlccEmis [4].

190

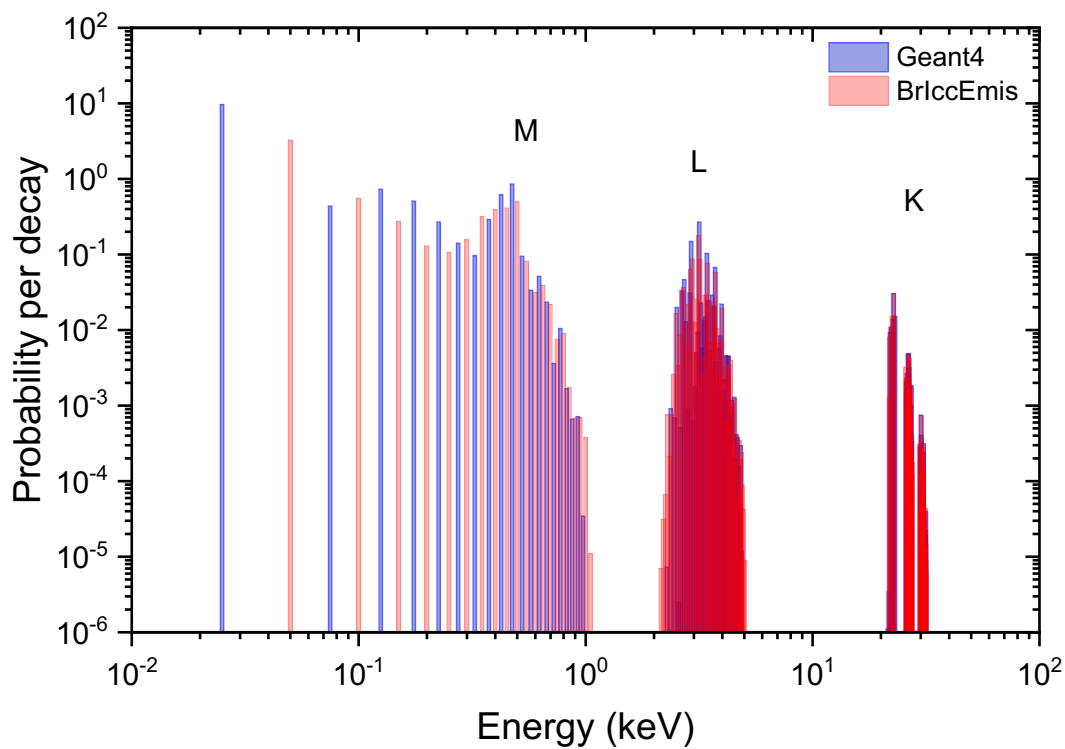


Fig. 2 Calculated Auger electron spectrum following the radioactive decay of ^{123}I , normalized for 1 radioactive decay. K, L and M indicate the major Auger groups.

191

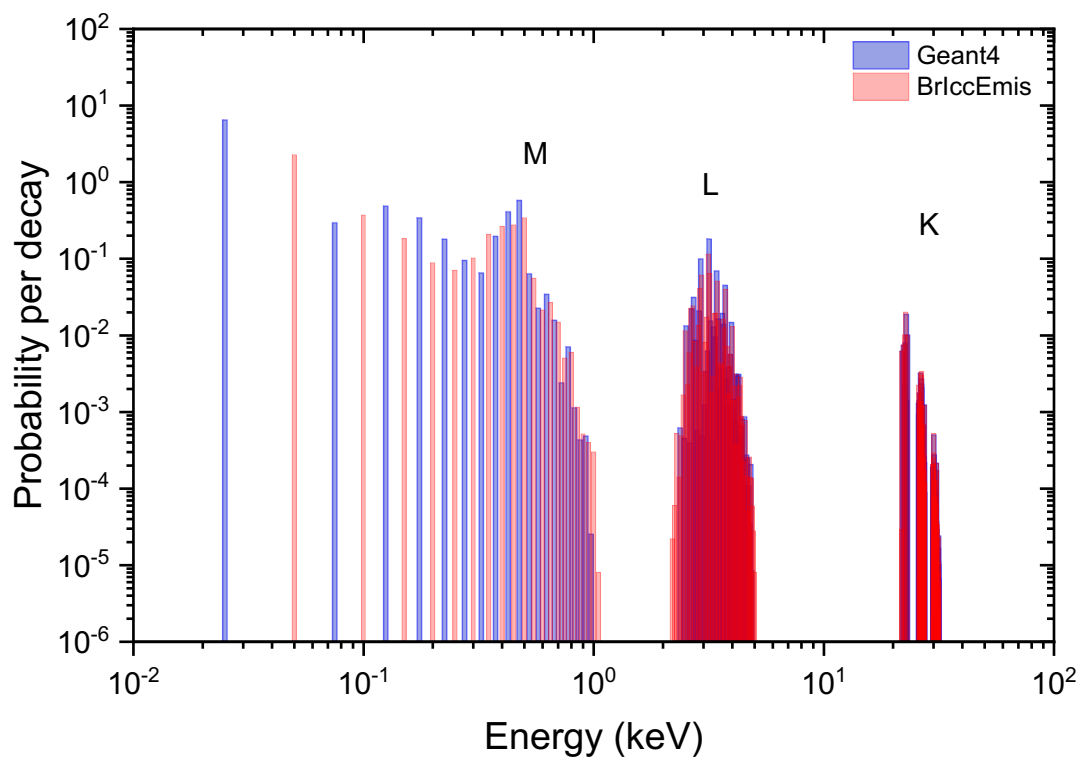


Fig. 3 Calculated Auger electron spectrum following the radiative decay of ^{124}I , normalized for 1 radioactive decay.

192

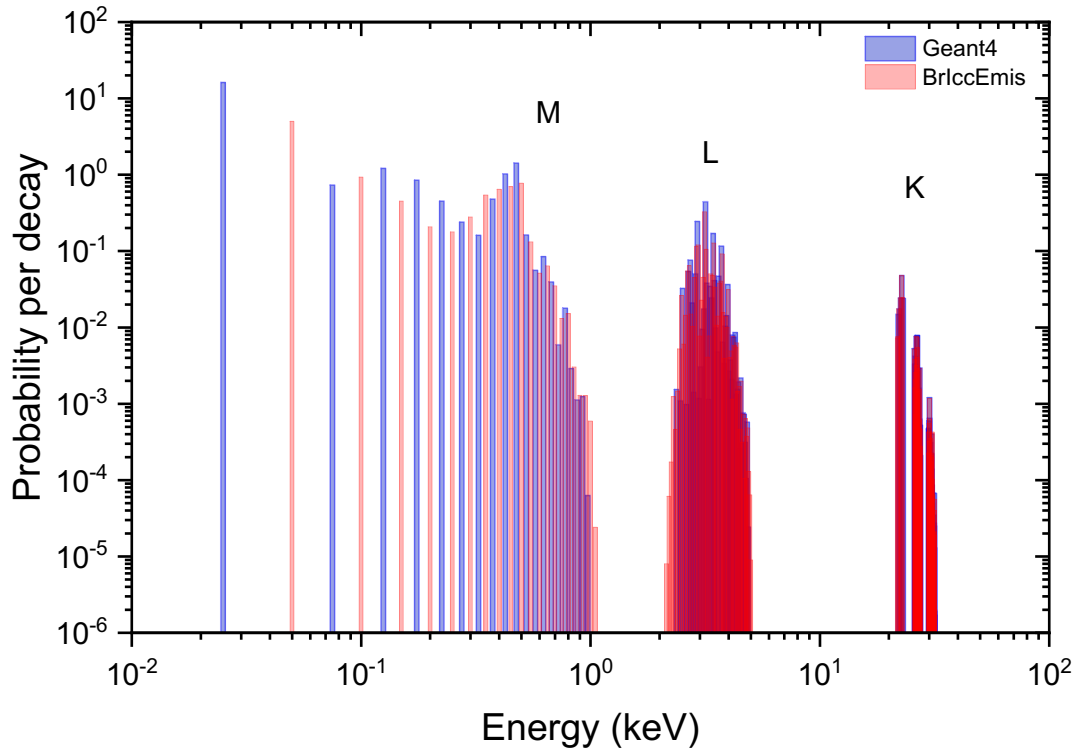


Fig. 4 Calculated Auger electron spectrum following the radiative decay of ^{125}I , normalized for 1 radioactive decay.

193

194 Tables 3, 4 and 5 show the Auger electron energies and emission yields for ^{123}I , ^{124}I and ^{125}I
 195 decay, respectively, as calculated by means of the Geant4 simulation described in section 2.3,
 196 the Geant4Lib analytical code, BrIccEmis [4], Pomplun [45] and Stepanek [27].

197

198 *Table 3. Mean Auger electron energies and emission yields per decay calculated for ^{123}I . \bar{E}*
 199 *is the mean energy of the transition as calculated in equation 1.*

Line	Geant4 simulation		Geant4Lib Analytical Code		BrIccEmis [4]		Pomplun [45]	
	\bar{E} (keV)	Yield	\bar{E} (keV)	Yield	\bar{E} (keV)	Yield	\bar{E} (keV)	Yield
Auger MXY	0.435	2.286	0.453	1.946	0.411	1.94	0.394	1.93
Auger LMM	3.067	0.653	3.085	0.734	3.047	0.733	3.028	0.711
Auger LMX	3.565	0.305	3.679	0.208	3.675	0.206	3.656	0.200
Auger KLL	22.666	0.0807	22.665	0.0807	22.525	0.0805	22.52	0.0731
Auger KLX	26.505	0.0355	26.506	0.0355	26.456	0.0354	26.43	0.0328
Auger KXY	30.348	0.00375	30.346	0.00374	30.312	0.00362	30.30	0.00280
Auger total	0.499	14.89	0.529	13.67	0.933	7.39	-	7.3
Auger above 500 eV	-	1.30	-	1.29	-	1.27	-	-

200

201 *Table 4. Mean Auger electron energies and emission yields per decay calculated for ^{124}I . \bar{E}*
 202 *is the mean energy of the transition as calculated in equation 1.*

Line	Geant4 simulation		Geant4Lib Analytical Code		BrIccEmis [4]	
	\bar{E} (keV)	Yield	\bar{E} (keV)	Yield	\bar{E} (keV)	Yield
Auger MXY	0.435	1.533	0.453	1.306	0.413	1.30
Auger LMM	3.086	0.491	3.085	0.492	3.048	0.492
Auger LMX	3.680	0.135	3.679	0.139	3.676	0.138
Auger KLL	22.666	0.0538	22.665	0.0541	22.525	0.0539

Auger KLX	26.506	0.0239	26.506	0.0238	26.460	0.0240
Auger KXY	30.348	0.00250	30.346	0.00251	30.308	0.00256
Auger total	0.499	9.99	0.528	9.17	0.922	5.04
Auger above 500 eV	-	0.87	-	0.87	-	0.85

203

204 *Table 5. Mean Auger electron energies and emission yields per decay calculated for ¹²⁵I. \bar{E} is*
 205 *the mean energy of the transition as calculated in equation 1 and Yield is Y_{total} of eq. 1.*

Line	Geant4 simulation		Geant4Lib Analytical Code		BrIccEmis [4]		Stepanek [27]	
	\bar{E} (keV)	Yield	\bar{E} (keV)	Yield	\bar{E} (keV)	Yield	\bar{E} (keV)	Yield
Auger MXY	0.435	3.800	0.453	3.224	0.408	3.20	0.380	3.24
Auger LMM	3.093	1.228	3.090	1.218	3.047	1.21	3.01	1.22
Auger LMX	3.692	0.331	3.684	0.345	3.676	0.339	3.63	0.339
Auger KLL	22.666	0.1286	22.665	0.129	22.522	0.129	22.6	0.126
Auger KLX	26.506	0.0568	26.506	0.0566	26.454	0.0565	26.5	0.0580
Auger KXY	30.349	0.00604	30.346	0.00597	30.322	0.00595	30.3	0.00550
Auger total	0.490	24.85	0.519	22.81	0.953	11.8	-	8.92
Auger above 500 eV	-	2.15	-	2.14	-	2.08	-	-

206

207 In reference to Fig. 2, 3 and 4, the Auger electron lines can be separated according to the
 208 atomic shell of the initial vacancy: above 20 keV for the K-shell, 2–5 keV for the L-shells, 0.2–
 209 1 keV for the M-shells, and below 0.2 keV for the remaining outer electron shells. It can be
 210 observed that the Auger electrons spectra calculated with Geant4 and BrIccEmis are similar
 211 from 500 eV to higher energies. For lower energies, the two theoretical approaches show
 212 differences in the calculation of the yields. In particular, Geant4 calculates higher Auger yields
 213 than BrIccEmis for all the radionuclides considered. It was also noticed that the major
 214 contribution to Auger emissions with energy below ~500 eV derives from N shell transitions.
 215 These discrepancies between the two theoretical approaches should be compared with
 216 absolute N-shell Auger electron transition rates, however we are not aware of the existence
 217 of suitable experimental data.

218 Table 3 shows the Auger electron energies and emission yields for ¹²³I decay as calculated by
 219 means of BrIccEmis [4], Pomplun [45] and Geant4. Geant4 calculates by default the full decay

220 chain, therefore the decay of ^{123}Te was switched off in the simulation, in order to compare
221 the same physical quantity against the other data. The Geant4 simulation results agree with
222 the Geant4Lib analytical code data in terms of Auger electron kinetic energies and in terms of
223 radiation yields with 4%, apart from the case of the radiation yield of the MXY, LMM and LMX
224 lines (17%, 11% and 46% of difference, respectively). This difference is ascribed to the
225 difficulty to identify the yields of specific lines in the Geant4 simulation using the methodology
226 described in 2.3 because of the overlapping of some group lines (see Figure 1). Apart from
227 this discrepancy, the results show consistency between the Geant4 simulation output and the
228 Geant4 data libraries used as input to describe Auger emission from radioactive decay, as
229 expected.

230 In terms of both energy and radiation yield, BrIccEmis [4] agrees within 1% with the Geant4
231 data libraries, apart from the case of Auger electron kinetic energies of MXY line where an
232 agreement within 9% has been observed and from the case of the radiation yield of the KXY
233 line where a difference of 5% was found. For Pomplun [45], an agreement within 2% with
234 Geant4 data libraries was found in terms of Auger electron kinetic energies, apart from 12%
235 difference for MXY line. In terms of radiation yield, there is an agreement within 10% apart
236 from the case of the KXY line where a difference of 25% was found. The total emission yield
237 above 500 eV shows a very good agreement for Geant4Lib analytical code and Geant4
238 simulation (within 1%) and BrIccEmis [4] (within 2%).

239 Table 4 displays the Auger electron energies and emission yields for ^{124}I decay calculated by
240 means of Geant4 and BrIccEmis [4]. The Geant4 simulation results agree with the Geant4Lib
241 analytical code data in terms of Auger electron kinetic energies within 1% for all lines, apart
242 from the case of MXY line where an agreement within 5% was found. In terms of emission
243 yields, Geant4 simulation results are consistent with Geant4Lib analytical code, apart from a
244 17% difference for the MXY line. As in the case of ^{123}I , we ascribe the difference to the
245 difficulty to determine the transition line (see Section 2.3 and Figure 1), complicated by the
246 overlapping of the Auger emission energies. BrIccEmis [4] agrees with Geant4 data libraries
247 within 1%, apart from the case of MXY line where an agreement within 8% has been observed.
248 With regard to the total emission yield above 500 eV, there is excellent agreement between
249 the Geant4 simulation and the Geant4Lib analytical code (within 0.5%), as expected.
250 Agreement within 3% was found between the Geant4 data libraries and BrIccEmis [4].

251 Table 5 reports the Auger electron energies and emission yields for ^{125}I decay calculated by
252 means of Geant4, BrIccEmis [4] and Stepanek [27]. In terms of Auger electron energy, Geant4
253 simulation results agree within 1 % with the Geant4 data libraries, apart from the case of the
254 MXY line (within 5%) and the total Auger electron emission. The differences are ascribed to
255 the difficulty to identify some lines (see Fig. 1), which is further complicated by a slight
256 broadening of the Auger electrons kinetic energies due to the momentum transfer to the
257 nuclear recoil. The Geant4 data libraries agree with BrIccEmis within 1% apart from the MXY
258 line (10%) and when considering the full spectrum of the Auger electrons. In terms of emission
259 yields, Geant4 simulation results are consistent with the Geant4Lib analytical code apart from
260 the case of MXY line, where differences up to 18% have been observed. This difference again
261 should be due to the method to distinguish the transition lines in the Geant4 simulation.
262 BrIccEmis [4] agrees with Geant4 data libraries within 2%. Besides, Stepanek [27] agrees
263 within 3% with Geant4 data libraries, while 17% difference has been noticed in terms of Auger
264 electron kinetic energies. In the matter of the total emission yield above 500 eV, there was
265 an excellent agreement (within 0.5%) between the Geant4 data libraries and the Geant4

266 simulation. An agreement within 3% was found between the Geant4 data libraries and
 267 BrlccEmis [4].

268 These results show, as expected, agreement between the Geant4 simulation and the
 269 Geant4Lib analytical code. Eventual disagreement is ascribed to the difficulty to identify the
 270 yields of specific lines in the Geant4 simulation. In addition, the results show an agreement
 271 within few percent between BrlccEmis [4], Stepanek [27] data and the Geant4Lib analytical
 272 code. Pomplun [45] data show less agreement with Geant4 and BrlccEmis [4].

273 **3.2. Comparison with experimental data**

274 Fig. 5 shows the yield per ^{125}I decay for K Auger electrons using Geant4, BrlccEmis [4] and
 275 Pomplun [26] data compared with the experimental results performed at ANU [8]. Fig. 6
 276 shows the ratio of the Auger electron emission yield calculated by either Geant4 or BrlccEmis
 277 [4] and the experimental results [8]. Fig. 7 shows the comparison of the Auger electron
 278 emission yield of ^{131}Cs decay calculated by means of Geant4, BrlccEmis [4] and the
 279 experimental data [43]. Fig. 8 illustrates the ratio of the emission yields calculated by either
 280 Geant4 simulation or BrlccEmis [4] and the experimental results [43].

281

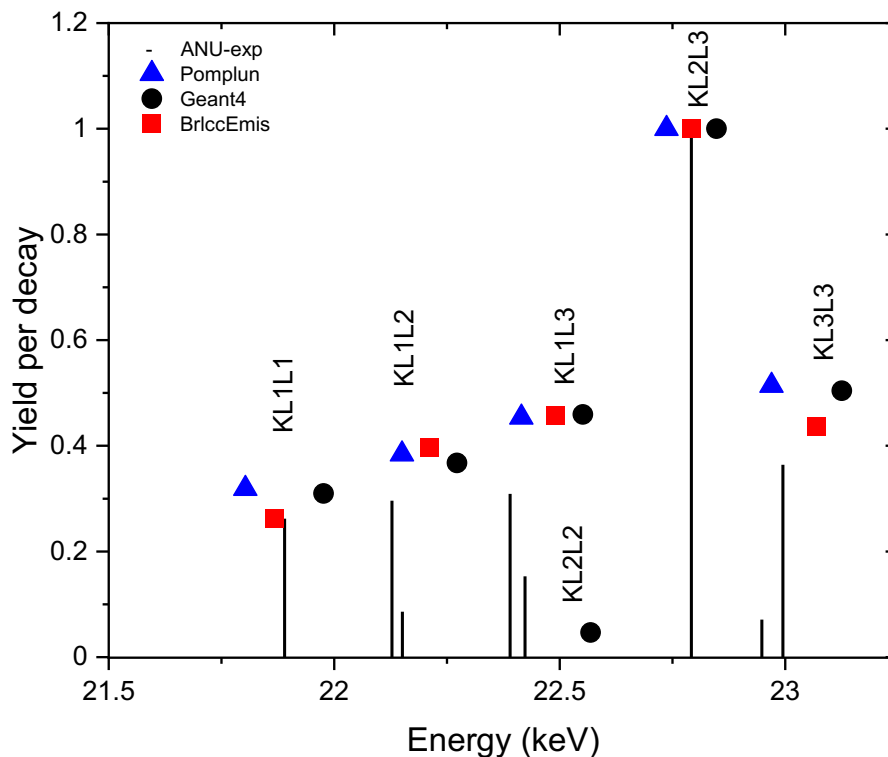


Fig. 5 Comparison of the Auger electron yields calculated by means of Geant4, BrlccEmis [4], and Pomplun [26] with experimental data [8] for KLL peaks in the case of ^{125}I decay.

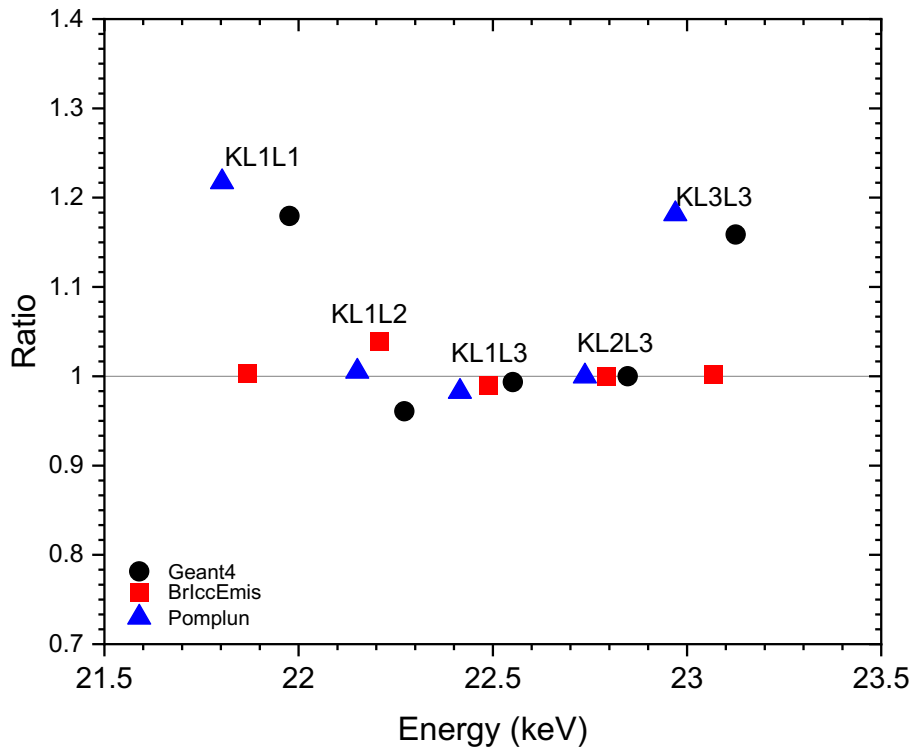


Fig. 6 Ratio of the Auger emission yield calculated by means of either Geant4, BrlccEmis [4], and Pomplun [26] and the experimental data [8]. The ratio has been calculated for KLL peaks in the case of ¹²⁵I decay.

284 Table 6. ¹²⁵I Auger electron yield calculated by means of Geant4, BrlccEmis [4], [8], Pomplun
 285 [26] and experimental data [8]. The experimental energy data have an uncertainty of around
 286 10 eV. The intensities are normalised to the KL2L3 line.

Line	Geant4 simulation		Geant4Lib Analytical Code		BrlccEmis [4]		Pomplun [26]		Experimental [8]	
	Energy (keV)	Yield	Energy (keV)	Yield	Energy (keV)	Yield	Energy (keV)	Yield	Energy (keV)	Yield
KL1L1(¹ S ₀)	21.9765	0.309	21.9765	0.309	21.868	0.263	21.803	0.319	21.800(5)	0.262(5)
KL1L2(¹ P ₁)	22.2725	0.367	22.2725	0.367	22.210	0.397	22.151	0.384	22.128(5)	0.296(10)
KL1L2(³ P ₀)									22.151(10)	0.086(6)
KL1L3(³ P ₁)	22.5515	0.459	22.5515	0.460	22.490	0.457	22.415	0.454	22.390(5)	0.309(7)
KL1L3(³ P ₂) + KL2L2(¹ S ₀)	22.5685	0.047	22.5685	0.047					22.423(5)	0.153(6)
KL2L3(¹ D ₂)	22.8475	1.000	22.8475	1.000	22.792	1.000	22.737	1.000	22.702(3)	1.000

KL3L3(³ P ₀)	23.1255	0.504	23.1255	0.504	23.068	0.436	22.970	0.514	22.948(10)	0.071(6)
KL3L3(³ P ₂)									22.995(4)	0.364(7)

287

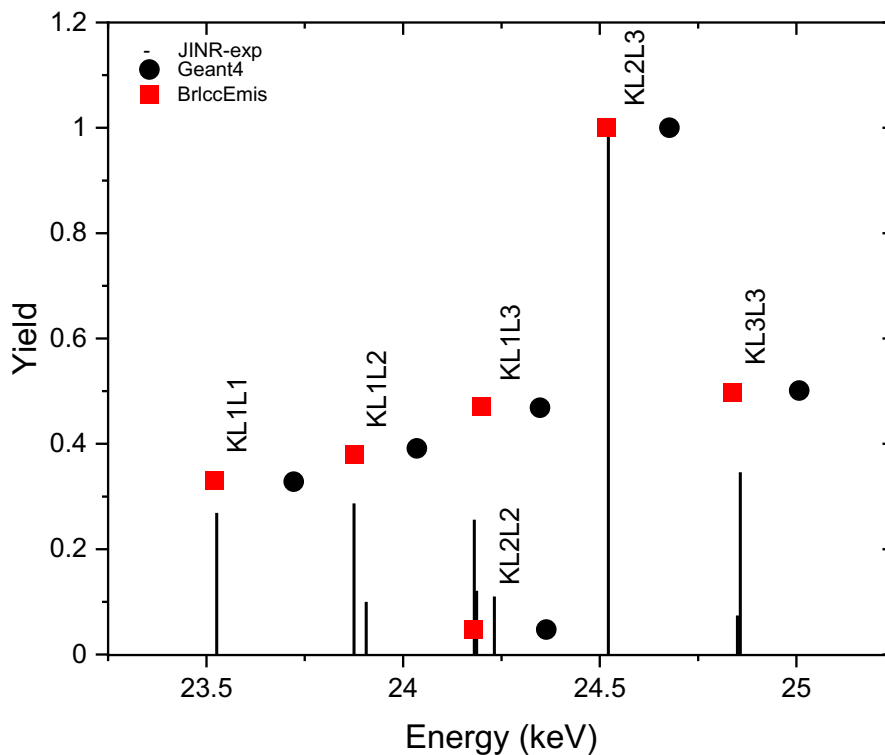


Fig. 7 Comparison of the Auger electron yields calculated by means of Geant4 and BrlccEmis [4] with experimental data [43] for Auger electron KLL peaks produced by ¹³¹Cs decay.

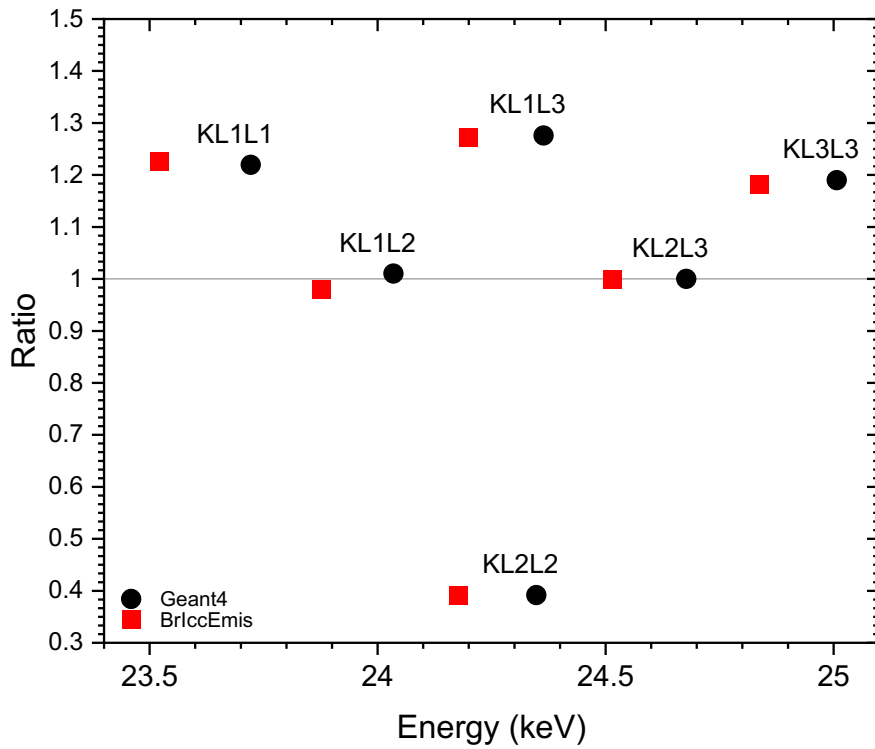


Fig. 8 Emission yield's ratio calculated dividing the results obtained with either Geant4 or BrlccEmis [4] and the experimental data [43]. The ratios are shown for Auger electron KLL peaks produced by ¹³¹Cs decay.

Table 7. ¹³¹Cs Auger electron yield calculated by means of Geant4 and BrlccEmis [46], and experimental yield [43].

Line	Geant4 simulation		Geant4Lib Analytical Code		BrlccEmis [46]		Experimental [43]	
	Energy (keV)	Yield	Energy (keV)	Yield	Energy (keV)	Yield	Energy (keV)	Yield
KL1L1(¹ S ₀)	23.722	0.328	23.722	0.329	23.521	0.330	23.526(6)	0.269(5)
KL1L2(¹ P ₁)	24.035	0.391	24.035	0.390	23.876	0.379	23.875(8)	0.287(5)
KL1L2(³ P ₀)							23.906(12)	0.100(5)
KL1L3(³ P ₁)	24.364	0.472	24.364	0.470	24.200	0.471	24.181(14)	0.256(41)
KL2L2(¹ S ₀)	24.348	0.047	24.348	0.048	24.178	0.047	24.187(18)	0.121(41)
KL1L3(³ P ₂)	-	-	-	-	-	-	24.232(10)	0.110(5)
KL2L3(¹ D ₂)	24.677	1.000	24.677	1.000	24.516	1.000	24.522(20)	1.000

KL3L3(3P_0)	25.007	0.501	25.007	0.500	24.838	0.498	24.850(12)	0.074(5)
KL3L3(3P_2)							24.857(6)	0.346(5)

292

293 Table 6 shows the ^{125}I Auger electron energies and yields obtained with Geant4 simulation,
 294 Geant4Lib analytical code, BrIccEmis [4] and Pomplun [26] models and the experimental data
 295 [8]. The experimental spectrum and theoretical peaks are scaled to match the intensity of the
 296 Geant4 KL2L3 Auger line. Good agreement in terms of Auger electron yield was found among
 297 Geant4, the experimental data and the other theoretical calculations. Geant4 simulations
 298 gave the same results of the Geant4Lib analytical code. Regarding to the emission yields of
 299 the experimental data [8] (see Fig. 5 and 6), an agreement within 15% (corresponding to the
 300 Geant4 model uncertainty) was found in comparison to Geant4 and 20% agreement with
 301 Pomplun [26]. In addition, a 5% agreement was found for BrIccEmis [4] in comparison to
 302 experimental data.

303 A comparison has been performed for the experimental KLL Auger energy spectrum deriving
 304 from the decay of ^{131}Cs , measured by Kovalik et al [43], with the theoretical one calculated
 305 using Geant4 simulation, Geant4Lib analytical code, and BrIccEmis [46]. The experimental
 306 spectrum and theoretical lines are scaled to match the intensity of the Geant4 KL2L3 Auger
 307 line. Table 7 displays the ^{131}Cs Auger electron energies and yields obtained with Geant4 and
 308 BrIccEmis [46] models and the experimental data. In terms of emission yields, good
 309 agreement (within 3%) was observed between Geant4 and BrIccEmis [46] theoretical
 310 calculations. Geant4 simulation results are consisted with the Geant4 data libraries. In Fig. 8,
 311 differences up to 25% were observed between Geant4 and BrIccEmis against the
 312 experimental data [43]. The only exception is the KL2L2 line, where a $\sim 250\%$ discrepancy has
 313 been noticed in comparison to the reference data [43], for both Geant4 and BrIccEmis.

314 In both comparisons (see Fig. 5 and 7), a kinetic energy shift (~ 150 eV) of the emission lines is
 315 observed for the Geant4 results. This most likely comes from the fact that Auger electron
 316 energies are derived from neutral binding energies (see Section 2.2). Moreover, the existing
 317 physics models describing atomic de-excitation of Geant4 disregard the quantum
 318 electrodynamics (QED) and Breit magnetic electron interaction corrections which could cause
 319 energy shift of the emitted Auger electrons and X-rays [46]. The QED effect is due to the fact
 320 that an electron moving in the vacuum drags a cloud of virtual photons with it [47], [48].
 321 BrIccEmis has semi-empirical correction for these effects.

322 Another difference in the model calculations is the atomic structure effect (~ 10 eV), which is
 323 only included in BrIccEmis and arises due to the fast vacancy cascade in the atom when it
 324 rearranges itself according to the atomic ground state of the daughter. This effect is important
 325 especially for transitions involving K and L shells where the vacancies have short lifetimes
 326 ($\sim 10^{-17} - 10^{-15}$ sec) [46].

327 4. Conclusion

328 In this work we benchmarked for the first time the emission of Auger electrons deriving from
 329 ^{123}I , ^{124}I , ^{125}I and ^{131}Cs decays calculated by means of Geant4 against other theoretical
 330 approaches (BrIccEmis [4], [46], Pomplun [26] and Stepanek [27]) and experimental results

331 performed at the Australian National University (ANU) [8] and the Joint Institute for Nuclear
332 Research (JINR) [43].

333 We verified the consistency between the Geant4 simulation results and the Geant4 data
334 libraries, input to the Monte Carlo code, to calculate Auger electron kinetic energies and
335 emission probabilities, deriving from atomic de-excitation after a radioactive decay.

336 When comparing Geant4 to other theoretical approaches, an overall good agreement, usually
337 within few percent in terms of Auger electron energies, was found between Geant4 and other
338 theoretical approaches. In terms of emission yields, a good agreement (within 3%) was found
339 for vacancies in the K shell. In the case of vacancies in the L and M shells, the level of
340 agreement was worse (within 15%) because it was difficult to determine the associated
341 transition lines in the Geant4 simulation. Overall, the total number of the Auger electron
342 emitted per radioactive decay was found significantly higher in Geant4. However, it was
343 noticed that the difference was mostly coming from the low energy range, below ~500 eV,
344 where the Auger electrons derive mainly from vacancies in N shell.

345 When comparing Geant4 simulation results to experimental data, a shift in the Auger kinetic
346 energies was found. This may be caused to limitations of the theoretical approach, which
347 considers the energy level of neutral atoms only and disregards quantum electrodynamics
348 (QED) effects, Breit magnetic electron interaction corrections and atomic structure effects.
349 These differences are not observed in the latest version of BrIccEmis [4], as it recently adopted
350 a semi-empirical correction, which reduces the difference between the calculated and
351 experimental Auger line energies below 10 eV [29].

352 In terms of Auger electron emission yields, once the results were normalised to KL2L3 line, an
353 agreement within 15% for ^{125}I and 25% ^{131}Cs radioactive decays, was found among Geant4,
354 BrIccEmis [4] and the measured K Auger intensity.

355 For the future, we recommend extending the benchmarking to the conversion lines, other
356 radioisotopes and to other sets of experimental measurements. As far as we know, this is the
357 first time that the Geant4 Auger emission from radioactive decay of medical radioisotopes
358 has been benchmarked against other theoretical approaches and validated against
359 experimental measurements.

360 **5. Acknowledgment**

361 This work has been funded by the Australian Research Council, grant number ARC
362 DP170100967 and DP140103317.

363 **6. References**

- 364 [1] B. Cornelissen and K. A. Vallis, "Targeting the Nucleus: An Overview of Auger-Electron Radionuclide
365 Therapy," *Curr. Drug Discov. Technol.*, vol. 7, no. 4, pp. 263–279, 2010.
- 366 [2] R. W. Howell, "Auger processes in the 21st century," vol. 84, no. 12, pp. 959–975, 2012.
- 367 [3] B. Q. Lee, T. Kibédi, and A. E. Stuchbery, "Auger yield calculations for medical radioisotopes," *EPJ Web*
368 *Conf.*, vol. 91, p. 00007, 2015.
- 369 [4] B. Q. Lee, H. Nikjoo, J. Ekman, P. Jonsson, A. E. Stuchbery, and T. Kibedi, "A stochastic cascade model
370 for Auger-electron emitting radionuclides," *Int J Radiat Biol*, vol. 92, no. 11, pp. 641–653, 2016.
- 371 [5] B. M. Bavelaar, B. Q. Lee, M. R. Gill, N. Falzone, and K. A. Vallis, "Subcellular targeting of theranostic
372 radionuclides," *Front. Pharmacol.*, vol. 9, no. SEP, pp. 1–17, 2018.

- 373 [6] A. I. Kassis, "The amazing world of Auger electrons," *Int. J. Radiat. Biol.*, vol. 80, no. 11–12, pp. 789–
374 803, Jan. 2004.
- 375 [7] A. M. S. Braghirolli, W. Waissmann, J. B. Da Silva, and G. R. Dos Santos, "Production of iodine-124 and
376 its applications in nuclear medicine," *Appl. Radiat. Isot.*, vol. 90, pp. 138–148, 2014.
- 377 [8] M. Alotiby *et al.*, "Measurement of the intensity ratio of Auger and conversion electrons for the
378 electron capture decay of ^{125}I ," *Phys. Med. Biol.*, vol. 63, no. 6, pp. 1–9, 2018.
- 379 [9] P. Balagurumorthy, X. Xu, K. Wang, S. J. Adelstein, and K. Amin I., "Effect of distance between
380 decaying ^{125}I and DNA on Augerelectron induced double-strand break yield," vol. 71, no. 2, pp. 233–
381 236, 2013.
- 382 [10] GEANT4-Collaboration, "Physics Reference Manual," *GEANT4 A Simul. toolkit - Man.*, vol. 1, pp. 1–554,
383 2019.
- 384 [11] P. Arce *et al.*, "Report on G4-Med, a Geant4 benchmarking system for medical physics applications
385 developed by the Geant4 Medical Simulation Benchmarking Group," *Med. Phys.*, 2020.
- 386 [12] S. Incerti, M. Douglass, S. Penfold, S. Guatelli, and E. Bezak, "Review of Geant4-DNA applications for
387 micro and nanoscale simulations," *Phys. Medica*, vol. 32, no. 10, pp. 1187–1200, Oct. 2016.
- 388 [13] C. Y. Huang, S. Guatelli, B. M. Oborn, and B. J. Allen, "Microdosimetry for targeted alpha therapy of
389 cancer," *Comput. Math. Methods Med.*, vol. 2012, 2012.
- 390 [14] C.-Y. Huang, B. M. Oborn, S. Guatelli, and B. J. Allen, "Monte Carlo calculation of the maximum
391 therapeutic gain of tumor antivascular alpha therapy," *Med. Phys.*, vol. 39, no. 3, pp. 1282–1288, Mar.
392 2012.
- 393 [15] S. Ohya, "Nuclear Data Sheets for $A = 123$," *Nucl. Data Sheets*, vol. 102, no. 3, pp. 547–718, 2004.
- 394 [16] J. Katakura and Z. D. Wu, "Nuclear Data Sheets for $A = 124$," *Nucl. Data Sheets*, vol. 109, no. 7, pp.
395 1655–1877, Jul. 2008.
- 396 [17] J. Katakura, "Nuclear Data Sheets for $A = 125$," *Nucl. Data Sheets*, vol. 112, no. 3, pp. 495–705, 2011.
- 397 [18] Y. Khazov, I. Mitropolsky, and A. Rodionov, "Nuclear Data Sheets for $A = 131$," *Nucl. Data Sheets*, vol.
398 107, no. 11, pp. 2715–2930, Nov. 2006.
- 399 [19] S. Incerti *et al.*, "Simulation of Auger electron emission from nanometer-size gold targets using the
400 Geant4 Monte Carlo simulation toolkit," *Nucl. Instruments Methods Phys. Res. Sect. B Beam Interact.*
401 *with Mater. Atoms*, vol. 372, no. Supplement C, pp. 91–101, 2016.
- 402 [20] S. Guatelli, A. Mantero, B. Mascialino, P. Nieminen, and M. G. Pia, "Geant4 Atomic Relaxation," *IEEE*
403 *Trans. Nucl. Sci.*, vol. 54, no. 3, pp. 585–593, 2007.
- 404 [21] S. T. Perkins, D. E. Cullen, M. H. Chen, J. Rathkopf, J. Scofield, and J. H. Hubbell, "Tables and Graphs of
405 Atomic Subshell and Relaxation Data Derived from the LLNL Evaluated Atomic Data Library, $Z=1$ -
406 100," *Eadl*, vol. 30, p. UCRL-50400, 1991.
- 407 [22] A. Mantero *et al.*, "PIXE simulation in Geant4," *X-Ray Spectrom.*, vol. 40, no. 3, pp. 135–140, 2011.
- 408 [23] W. Bambynek *et al.*, "Orbital electron capture by the nucleus," *Rev. Mod. Phys.*, vol. 49, no. 1, pp. 77–
409 221, Jan. 1977.
- 410 [24] T. Kibédi, T. W. Burrows, M. B. Trzhaskovskaya, P. M. Davidson, and C. W. Nestor, "Evaluation of
411 theoretical conversion coefficients using Brlcc," *Nucl. Instruments Methods Phys. Res. Sect. A Accel.*
412 *Spectrometers, Detect. Assoc. Equip.*, vol. 589, no. 2, pp. 202–229, 2008.
- 413 [25] R. Jenkins, R. Manne, R. Robin, and C. Senemaud, "IUPAC—nomenclature system for x-ray
414 spectroscopy," *X-Ray Spectrom.*, vol. 20, no. 3, pp. 149–155, 1991.
- 415 [26] E. Pomplun, "Auger Electron Spectra - The Basic Data for Understanding the Auger Effect," *Acta Oncol.*
416 *(Madr.)*, vol. 39, no. 6, pp. 673–679, 2000.
- 417 [27] J. Stepanek, "Methods to determine the fluorescence and Auger spectra due to decay of radionuclides
418 or due to a single atomic-subshell ionization and comparisons with experiments," *Med. Phys.*, vol. 27,

- 419 no. 7, pp. 1544–1554, 2000.
- 420 [28] B. Q. Lee, T. Kibédi, A. E. Stuchbery, and K. A. Robertson, “Atomic radiations in the decay of medical
421 radioisotopes: A physics perspective,” *Comput. Math. Methods Med.*, vol. 2012, 2012.
- 422 [29] B. P. E. Tee, T. Kibédi, B. Q. Lee, M. Vos, R. du Rietz, and A. E. Stuchbery, “Development of a new
423 database for Auger electron and X-ray spectra,” *EPJ Web Conf.*, vol. 232, p. 01006, 2020.
- 424 [30] “Evaluated Nuclear Structure Data File.” [Online]. Available: <https://www.nndc.bnl.gov/ensdf/>.
- 425 [31] A. Endo, Y. Yamaguchi, and K. F. Eckerman, “Nuclear Decay Data for Dosimetry Calculations: Revised
426 Data of ICRP Publication 38,” vol. Supplement, 2005.
- 427 [32] N. B. Gove and M. J. Martin, “Log-f tables for beta decay,” *At. Data Nucl. Data Tables*, vol. 10, no. 3, pp.
428 205–219, Nov. 1971.
- 429 [33] M. J. Martin and P. H. Blichert-toft, “Radioactive atoms: Auger-Electron, α -, β -, γ -, and X-Ray Data,” *At.
430 Data Nucl. Data Tables*, vol. 8, no. 1–2, pp. 1–198, Oct. 1970.
- 431 [34] E. Schönfeld, “Calculation of fractional electron capture probabilities,” *Appl. Radiat. Isot.*, vol. 49, no.
432 9–11, pp. 1353–1357, Aug. 1998.
- 433 [35] L. Storm and H. I. Israel, “Photon cross sections from 1 keV to 100 MeV for elements Z=1 to Z=100,” *At.
434 Data Nucl. Data Tables*, vol. 7, no. 6, pp. 565–681, 1970.
- 435 [36] M. H. Chen, B. Crasemann, and H. Mark, “Relativistic radiationless transition probabilities for atomic K-
436 and L-shells,” *At. Data Nucl. Data Tables*, vol. 24, no. 1, pp. 13–37, Jul. 1979.
- 437 [37] E. J. McGuire, “ $\text{K}\alpha$ -Shell Auger Transition Rates and Fluorescence Yields for Elements Be-Ar,” *Phys.
438 Rev.*, vol. 185, no. 1, pp. 1–6, Sep. 1969.
- 439 [38] J. H. Scofield, “Relativistic hartree-slater values for K and L X-ray emission rates,” *At. Data Nucl. Data
440 Tables*, vol. 14, no. 2, pp. 121–137, Aug. 1974.
- 441 [39] J. P. Desclaux, “Relativistic Dirac-Fock expectation values for atoms with Z = 1 to Z = 120,” *At. Data
442 Nucl. Data Tables*, vol. 12, no. 4, pp. 311–406, Jan. 1973.
- 443 [40] I. M. Band, M. B. Trzhaskovskaya, C. W. Nestor, P. O. Tikkanen, and S. Raman, “Dirac-fock internal
444 conversion coefficients,” *At. Data Nucl. Data Tables*, vol. 81, no. 1–2, pp. 1–334, 2002.
- 445 [41] A. Pronschinske *et al.*, “Enhancement of low-energy electron emission in 2D radioactive films,” *Nat.
446 Mater.*, vol. 14, no. 9, pp. 904–907, 2015.
- 447 [42] M. Alotiby, I. Greguric, T. Kibédi, B. Tee, and M. Vos, “Quantitative electron spectroscopy of ^{125}I over
448 an extended energy range,” *J. Electron Spectros. Relat. Phenomena*, vol. 232, pp. 73–82, 2019.
- 449 [43] A. Kovalik *et al.*, “The electron spectrum from the atomic deexcitation of $\text{Xe-}^{131}(54)$,” *J. Electron
450 Spectros. Relat. Phenomena*, vol. 95, no. 2–3, pp. 231–254, 1998.
- 451 [44] C. Briançon, B. Legrand, R. J. Walen, T. Vylov, A. Minkova, and A. Inoyatov, “A new combined
452 electrostatic electron spectrometer,” *Nucl. Instruments Methods Phys. Res.*, vol. 221, no. 3, pp. 547–
453 557, Apr. 1984.
- 454 [45] E. Pomplun, “Monte Carlo-simulated Auger electron spectra for nuclides of radiobiological and medical
455 interest – a validation with noble gas ionization data,” *Int. J. Radiat. Biol.*, vol. 88, no. 1–2, pp. 108–114,
456 Jan. 2012.
- 457 [46] B. Lee, “A Numerical Model of Atomic Relaxation and its Applications,” The Australian National
458 University, 2017.
- 459 [47] P. Milonni, *An Introduction to Quantum Electrodynamics*, 1994th ed. Boston: Academic Press, Boston.
- 460 [48] T. Rentrop, A. Trautmann, F. A. Olivares, F. Jendrzewski, A. Komnik, and M. K. Oberthaler,
461 “Observation of the phononic Lamb shift with a synthetic vacuum,” *Phys. Rev. X*, vol. 6, no. 4, pp. 1–10,
462 2016.
- 463